THYROID
Volume 29, Number 2, 2019

DOI: 10.1089/thy.2018.0791

SPECIAL ARTICLE

GLIS Rearrangement is a Genomic Hallmark of Hyalinizing Trabecular Tumor of the Thyroid Gland

Marina N. Nikiforova,[1] Alyaksandr V. Nikitski,[1] Federica Panebianco,[1] Cihan Kaya,[1] Linwah Yip,[2] Michelle Williams,[3] Simion I. Chiosea,[1] Raja R. Seethala,[1] Somak Roy,[1] Vincenzo Condello,[1] Lucas Santana-Santos,[1] Abigail I. Wald,[1] Sally E. Carty,[2] Robert L. Ferris,[4] Adel K. El-Naggar,[3] and Yuri E. Nikiforov[1]

Background: Hyalinizing trabecular tumor (HTT) is a rare thyroid neoplasm with a characteristic trabecular growth pattern and hyalinization. This lesion has been the subject of long-term controversy surrounding its genetic mechanisms, relationship to papillary thyroid carcinoma (PTC), and malignant potential. Due to the presence of nuclear features shared with PTC, HTT frequently contributes to a false-positive cytology, which hampers patient management. The goal of this study was to apply genome-wide sequencing analyses to elucidate the genetic mechanisms of HTT and its relationship to PTC.
Methods: Whole-exome, RNA-Seq, and targeted next-generation sequencing analyses were performed to discover and characterize driver mutations in HTT. RNA-Seq results were used for pathway analysis. Tissue expression of GLIS3 and other proteins was detected by immunohistochemistry. The prevalence of *GLIS* fusions was studied in 17 tumors initially diagnosed as HTT, 220 PTC, and 10,165 thyroid fine-needle aspiration samples.
Results: Using whole-exome and RNA-Seq analyses of the initial three HTT, no known thyroid tumor mutations were identified, while in-frame gene fusion between *PAX8* exon 2 and *GLIS3* exon 3 was detected in all tumors. Further analysis identified *PAX8–GLIS3* in 13/14 (93%) and *PAX8–GLIS1* in 1/14 (7%) of HTT confirmed after blind pathology review. The fusions were validated by Sanger sequencing and FISH. The fusions resulted in overexpression of the 3′-portion of GLIS3 and GLIS1 mRNA containing intact DNA-binding domains of these transcription factors and upregulation of extracellular matrix genes including collagen IV. Immunohistochemistry confirmed upregulation and deposition of collagen IV and pan-collagen in HTT. The analysis of 220 PTC revealed no *PAX8–GLIS3* and one *PAX8–GLIS1* fusion. *PAX8–GLIS3* was prospectively identified in 8/10,165 (0.1%) indeterminate cytology fine-needle aspiration samples; 5/5 resected fusion-positive nodules were HTT on surgical pathology.
Conclusions: This study demonstrates that *GLIS* rearrangements, particularly *PAX8–GLIS3*, are highly prevalent in HTT but not in PTC. The fusions lead to overexpression of GLIS, upregulation of extracellular matrix genes, and deposition of collagens, which is a characteristic histopathologic feature of HTT. Due to unique genetic mechanisms and an indolent behavior, it is proposed to rename this tumor as ''*GLIS*-rearranged hyalinizing trabecular adenoma.''

Keywords: GLIS3, GLIS1, thyroid, hyalinizing trabecular tumor

Introduction

Hyalinizing trabecular tumor (HTT) is a rare neoplasm derived from thyroid follicular cells that shows no invasion and has a characteristic trabecular growth pattern and hyalinization. This lesion has been the subject of long-term controversy surrounding its genetic mechanisms, relationship to papillary thyroid carcinoma (PTC), and malignant potential.

The first detailed description of this tumor in the modern era was provided by Carney *et al.*, who reported in 1987 a series of 11 tumors with distinct histopathological appearance and named them ''hyalinizing trabecular adenoma'' (1). All of these tumors had a prominent trabecular pattern, abundant intra-trabecular hyalinized stroma, and nuclear features overlapping with those of PTC, but they were well circumscribed or encapsulated, had no invasion, and demonstrated no tumor recurrence or metastasis on a 10-year

[1]Department of Pathology and [2]Division of Endocrine Surgery, University of Pittsburgh Medical Center, Pittsburgh, Pennsylvania.
[3]Department of Pathology, Division of Pathology/Lab Medicine, The University of Texas, MD Anderson Cancer Center, Houston, Texas.
[4]UPMC Hillman Cancer Center, UPMC Cancer Pavilion, Pittsburgh, Pennsylvania.

mean follow-up (1). A year later, the same tumor was described by Bronner *et al*. in a series of nine cases as ''paraganglioma-like adenoma of the thyroid'' (2).

In 1991, a study of nine thyroid tumors with trabecular pattern and hyalinization was reported, and one of those cases had a lymph node metastasis at presentation (3). Although the latter case was diagnosed on incisional biopsy only, the authors argued that tumors with such appearance may have malignant behavior and should be designated as ''hyalinizing trabecular tumor.'' Several subsequent studies reported rare tumors with trabecular appearance and hyalinization that were associated with blood vessel or tumor capsule invasion and distant metastasis, as well as areas of classic PTC merging with this tumor (4–6). Together with the prominent nuclear features of PTC seen in the tumor cells, these reports argued against the benign nature of hyalinizing trabecular adenoma. As the controversy persisted, the 2004 World Health Organization (WHO) classification placed this tumor in a separate category of tumors with low malignant potential and designated it as ''hyalinizing trabecular tumor'' (7). The same approach was followed by the most recent 2017 WHO classification of tumors of endocrine organs (8).

The biological relationship of this tumor to PTC was suggested by two publications reporting that HTT frequently harbor *RET/PTC* rearrangements (9,10), a characteristic genetic feature of PTC. However, these reports raised a controversy by themselves due to concerns about the histologic criteria for tumor selection and use of highly sensitive assays for *RET/PTC* detection prone to false positivity (11). A subsequent study revealed no *RET/PTC* rearrangements in a series of 18 HTT analyzed by reverse transcription polymerase chain reaction (RT-PCR) (12). Furthermore, these tumors were found to harbor no *BRAF* or *RAS* mutations, which are highly prevalent in classic type and follicular variant PTC (12–18), pointing to a possibility that HTT is a distinct tumor and not a variant of PTC.

The controversy was further fueled by the fact that HTT cells exhibit pronounced nuclear features of PTC, including nuclear pseudoinclusions, and are frequently diagnosed as either PTC or suspicious for PTC in fine-needle aspiration (FNA) cytology samples (19).

As a result, over the last 15 years, this lesion has been considered a borderline tumor with low malignant potential rather than a benign adenoma. This is despite the fact that no adverse outcome has ever been documented in a tumor with this morphology lacking invasive features at presentation (20).

The goal of this study was to apply genome-wide molecular analyses based on next-generation sequencing (NGS) to elucidate the genetic mechanisms of HTT and investigate its relationships with PTC.

Methods

Study samples

Snap-frozen tissue and formalin-fixed paraffin-embedded (FFPE) tissue samples collected at the Department of Pathology at the University of Pittsburgh Medical Center (UPMC) were retrospectively studied following approval by the University of Pittsburgh Institutional Review Board (IRB). Additional fresh-frozen tissue samples from HTT and corresponding normal thyroid were collected at the MD Anderson Cancer Center with IRB approval. Finally, retrospective analysis of genomic data from 10,165 consecutive FNA samples from thyroid nodules with indeterminate cytology routinely tested by ThyroSeq v3 Genomic Classifier (GC) was performed. Clinical and surgical follow-up was collected on 14 resected HTT and eight FNA samples positive for *GLIS* fusions.

Pathology review

Glass slides from tumors initially diagnosed as HTT at the Department of Pathology at the UPMC were reviewed by three thyroid pathologists (R.R.S., S.I.C., and Y.E.N.) blinded for the results of molecular analyses. All tumors were classified according to the 2017 WHO classification of endocrine tumors (8). In case of discrepancy of diagnostic opinion, cases were discussed again and a consensus diagnosis was reached.

Whole-exome sequencing

The library construction was performed using the SeqCap EZ System (NimbleGen, Madison, WI) according to the manufacturer's instructions. Briefly, genomic DNA was sheared, the size was selected to roughly 300 bp, and the ends were repaired and ligated to specific adapters and multiplexing indexes. Fragments were incubated with SeqCap biotinylated DNA baits after ligation-mediated PCR, and the hybrids were purified using streptavidin-coated magnetic beads. After amplification of ≤18 PCR cycles, the libraries were sequenced on the HiSeq 3000 (Illumina, San Diego, CA), using 100 bp pair-ended reads.

Bioinformatics analysis was performed using a custom protocol developed for tumor and paired normal and tumor-only analysis (21). Briefly, after conversion of base call files to FASTQ files using bcltofastq (Illumina), sequences were aligned to the human reference genome (GRCh37.p13; GCF_000001405.25) using BWA MEM (22) and encoded into a BAM (binary sequence alignment) format using Samtools (23). Post alignment, the BAM files were sorted, indexed, de-duplicated, and subjected to local indel realignment and base quality score recalibration using GATK (24). Subsequently, variant calling was performed using Varscan2 (25) for single nucleotide variants (SNV) and short indel detection and Scalpel (26) for large indel detection. Variant calls from both callers were integrated, normalized, annotated (27,28), and prioritized based on reported minor allele frequency in population databases (29,30), variant location (coding vs. non-coding), *in silico* prediction algorithms (31,32), and public somatic and germline variant databases (33–35). Somatic mutation density analysis was performed for samples with tumor and paired normal and included all non-synonymous SNV and small indels in the coding regions of the genes. Copy number and loss of heterozygosity analysis was performed using FACETS (36) and CNVkit (37) algorithms.

RNA-Seq analysis

For RNA-Seq (transcriptome) analysis, libraries were prepared using the Illumina TruSeq™ RNA Exome Sample Preparation Kit v1, according to the manufacturer's protocol. Cluster generation and paired-end sequencing were performed on an Illumina HiSeq2500 using a HiSeq Paired-End

(PE) Rapid Cluster Kit v2 and HiSeq Rapid SBS Lit v2 (Illumina).

For detection of gene fusions, the sequencing reads were collected, and a quality filtering was applied based on Q-score (38). The Chimerascan algorithm (39), which utilizes Tophat aligner (40), was used. The fusions detected with Chimerascan were filtered using custom filtering algorithm that utilizes the distance between breakpoints and various cancer databases, such as Atlas (41), CIS (RTCGD) (42), and CHCG (43). The junctions and the individual exon expression levels were used to visualize the fusion point.

For gene expression analysis, the filtered high-quality reads from HiSeq sequencing system were aligned to human genome (hg19-GRCh37) using TopHat aligner (40), and the number of reads mapped to each gene was calculated using RSeM (44) and featureCounts (45) tools. From the read counts, the differential expression analysis was performed using the edgeR package (46). The genes with a fold change >2 with a p-value of <0.05 were selected as differentially expressed genes and used in pathway analysis using various databases such as KEGG (47), Reactome (48), and DAVID (49). The GO biological process analysis was conducted using DAVID (49). The fold changes in GLIS3 and GLIS1 expression between *GLIS*-rearranged HTT and normal thyroid tissue were also analyzed using transcript counts (TPM) with the fold-change detection pipeline (50).

Targeted NGS

Targeted NGS analysis was performed to genotype surgically removed tissue samples and FNA samples from thyroid nodules with indeterminate cytology using the ThyroSeq v3 GC assay, as previously described (51). The assay uses targeted amplification-based NGS technology to detect genomic alterations in 112 thyroid-related genes, including *PAX8–GLIS3* fusion by sequencing DNA and RNA on the Ion GeneStudio S5 System (Thermo Fisher Scientific, Waltham, MA) according to the manufacturer's protocol. Torrent Suite software v5.2.2 (Thermo Fisher Scientific) and software developed in house (Variant Explorer v2) were used for data analysis and interpretation (51).

RT-PCR and Sanger sequencing analysis

RNA from frozen and FFPE tissues was reverse transcribed with the High Capacity cDNA Reverse Transcription Kit (Applied Biosystems, Foster City, CA) and by SuperScript IV VILO Master Mix (Invitrogen, Carlsbad, CA), respectively. RT-PCRs were conducted by HotStarTaq DNA Polymerase (Qiagen, Valencia, CA), using the primers reported in Supplementary Table S1. The RT-PCR products were sequenced in both directions using the BigDye Terminator Kit and an ABI 3130xl DNA Sequencer.

Fluorescence in situ *hybridization*

Following deparaffinization and rehydration, 4 μm FFPE sections were used to hybridize with commercially available probes from Empire Genomics LLC for PAX8 (green), GLIS3 (orange), and GLIS1 (orange) to detect *PAX8–GLIS3* or *PAX8–GLIS1* fusions. An additional PAX8 probe (green) was generated from BAC clone RP11-155L11 (Empire Genomics LLC, Buffalo, NY). Microscopy was performed using a Leica SP5 TCS 4D confocal laser scanning fluorescence microscope (Leica Camera, Wetzlar, Germany) with digital image capture.

Immunohistochemical analysis

After deparaffinization and rehydration, 4 μm FFPE sections were incubated with primary rabbit antibodies (anti-GLIS3, 1:50, NBP2-33787, Novus Biologicals, Centennial, CO; anti-pan-Collagen, 1:100, PA1-85324, Thermo Fisher Scientific; and anti-Collagen IV, 1:100, PA1-28534, Dako) for 14 hours at 4°C. Following the washes, secondary HRP-conjugated anti-rabbit antibodies (1:100; P0448; Dako, Agilent, Santa Clara, CA) were applied. Visualization was performed with DAB Peroxidase Substrate Kit (SK-4100; Vector Laboratories, Burlingame, CA).

Results

Identification of GLIS3 fusion in HTT using NGS

To search for driver genetic alterations in HTT, first whole-exome sequencing (WES) of DNA from three snap-frozen HTT samples and two corresponding normal tissues was performed. The analysis revealed no driver point mutations or indels known for thyroid or other cancer types and no potential novel driver mutations (Supplementary Table S2). Overall, the analysis showed a low somatic mutation density ($M = 0.039$ non-synonymous mutations/Mb) in the two tumors with corresponding normal tissue available. In addition, the WES analysis demonstrated absence of significant somatic DNA copy number alterations in these tumors (Supplementary Fig. S1).

Next, RNA-Seq (transcriptome) analysis of the three snap-frozen HTT samples and one corresponding normal tissue sample was performed. It detected an in-frame fusion between exon 2 of the *PAX8* gene and exon 3 of the *GLIS3* gene in all three HTT samples, while no fusion was identified in corresponding normal thyroid tissue (Supplementary Table S3). The fusion is expected to be a result of an inter-chromosomal rearrangement between the *PAX8* gene located on chromosome 2q14.1 and *GLIS3* on chromosome 9p24.2 (Fig. 1A). The fusions were confirmed in all HTT samples by RT-PCR and Sanger sequencing (Fig. 1 B). RT-PCR also showed the presence of alternative transcripts between *PAX8* exon 2 and *GLIS3* exon 4, which were not, however, in-frame. In addition to the *PAX8–GLIS3* fusion, two HTT samples revealed the presence of several intra-chromosomal fusions involving the 2q11.2–2q14.1 chromosomal region adjacent to the location of *PAX8* (Supplementary Table S3), providing evidence for multiple chromosomal breaks occurring in this region on 2q.

Analysis of an expanded cohort of HTT cases

To determine the prevalence of *PAX8–GLIS3* fusion in these tumors, 14 additional samples initially diagnosed as HTT were studied (Table 1). All samples were analyzed by RT-PCR, Sanger sequencing, and a 112-gene targeted NGS panel (ThyroSeq v3 GC) that detects *PAX8–GLIS3* and other gene fusions in addition to mutations and copy number alterations. Seven of those samples that had sufficient RNA quantities were studied by RNA-Seq. Overall, 10/14 samples

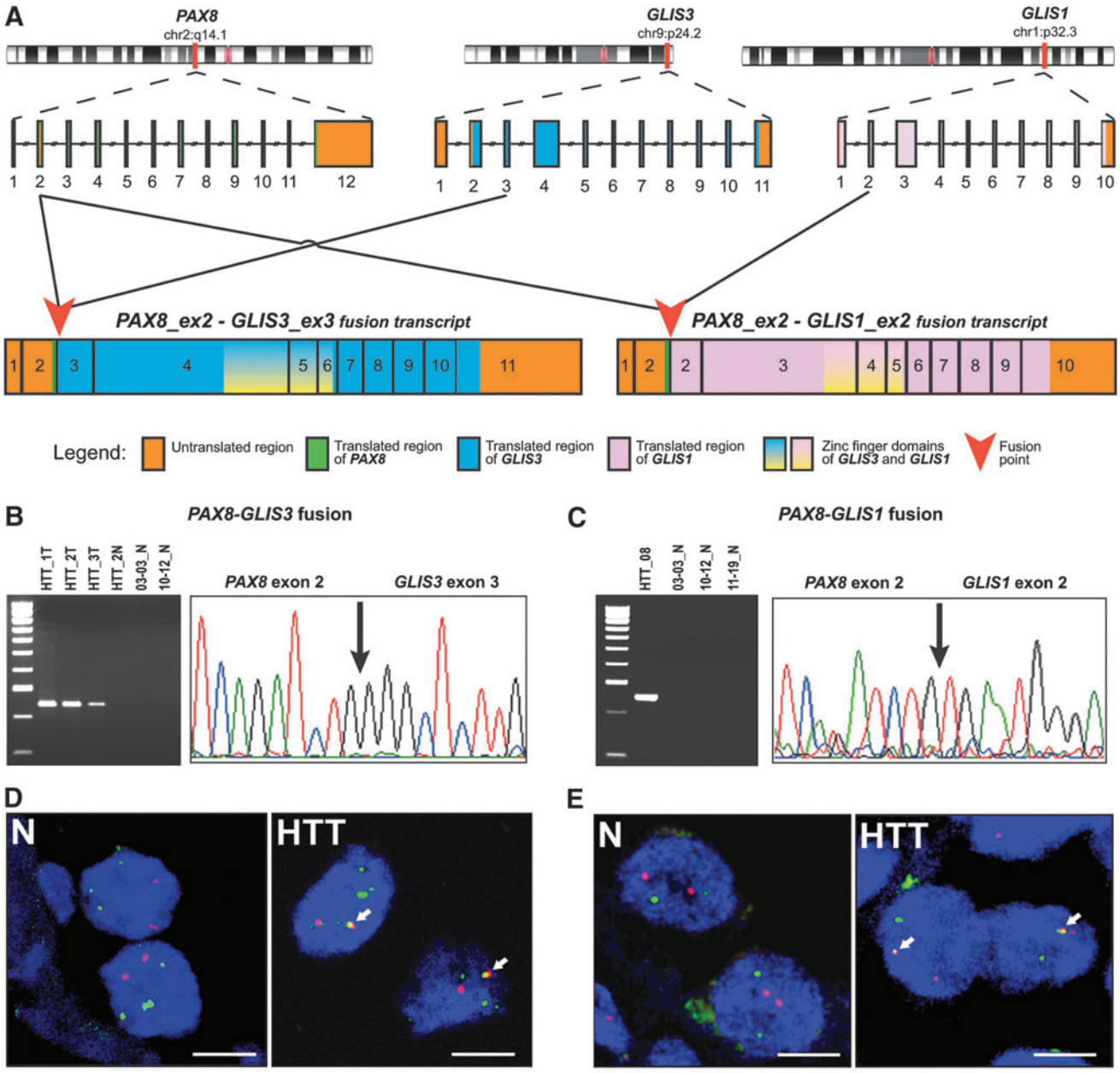

FIG. 1. Structure and confirmation of *PAX8–GLIS3* and *PAX8–GLIS1* fusions identified by RNA-Seq analysis in hyalinizing trabecular tumor (HTT) samples. (**A**) Schematic representation of the *PAX8*, *GLIS3*, and *GLIS1* genes and *PAX8–GLIS3* and *PAX8–GLIS1* fusion transcripts. (**B** and **C**) Reverse transcription polymerase chain reaction (left) and Sanger sequencing (right) confirmation of *PAX8–GLIS3* (**B**) and *PAX8–GLIS1* (**C**) fusions. (**D**) Fluorescence *in situ* hybridization (FISH) of normal thyroid tissue (N) and *PAX8–GLIS3* fusion-positive tumors (HTT) with *PAX8* (green) and *GLIS3* (orange) probes showing nuclei with separate signals in normal cells and one pair of fused signals in HTT cell nuclei (arrows). (**E**) FISH of normal thyroid tissue (N) and *PAX8–GLIS1* fusion-positive tumors (HTT) with *PAX8* (green) and *GLIS1* (orange) probes showing nuclei with separate signals in normal cells and one pair of fused signals in HTT cell nuclei (arrows). Additional small green signals are due to non-specific hybridization.

were found to be positive for the same fusion between exon 2 of the *PAX8* gene and exon 3 of *GLIS3*. No *BRAF*, *RAS*, or *RET/PTC* mutations or other driver fusions were identified in these samples. However, out of four *PAX8–GLIS3* fusion-negative cases, one was positive for the *HRAS* p.Q61R mutation, two were positive for multiple copy number alterations, and one sample was negative for all genomic alterations by targeted NGS analysis but revealed a *PAX8–GLIS1* fusion on RNA-Seq (Fig. 2). In the latter case, the fusion point of the chimeric transcript was between exon 2 of the *PAX8* gene and exon 2 of *GLIS1* (Fig. 1A). *PAX8* is located on chromosome 2q14.1 and *GLIS1* on chromosome 1p32.3, indicating that the fusion is a result of an inter-chromosomal rearrangement. The fusion was confirmed by RT-PCR and Sanger sequencing (Fig. 1C). Analysis of eight normal thyroid tissues available for these cases by targeted NGS revealed no *GLIS* fusions or

TABLE 1. CHARACTERISTICS OF TUMORS INITIALLY DIAGNOSED AS HTT

Study number	*Sex*	*Age (years)*	*Initial path diagnosis*	*Tumor size (cm)*	*Gene alterations detected*	*Consensus path diagnosis*
S01-HTT	F	50	HTT	1.1	PAX8/GLIS3	HTT
S02-HTT	F	55	HTT	1.3	PAX8/GLIS3	HTT
S03-HTT	F	44	HTT	0.7	PAX8/GLIS3	HTT
S04-HTT	F	70	HTA	2.5	PAX8/GLIS3	HTT
S05-HTT	F	60	HTT	0.6	PAX8/GLIS3	HTT
S06-HTT	F	44	HTT	0.7	PAX8/GLIS3	HTT
S07-HTT	F	60	HTT	3.5	PAX8/GLIS3	HTT
S08-HTT	F	55	HTT	0.8	PAX8/GLIS1	HTT
S09-HTT	F	69	HTT	3.2	PAX8/GLIS3	HTT
S10-HTT	F	59	HTT	1.0	PAX8/GLIS3	HTT
S11-HTT	F	31	HTT	2.3	PAX8/GLIS3	HTT
S12-HTT	F	58	HTT	2.0	PAX8/GLIS3	HTT
S13-HTT	F	68	HTT	0.9	PAX8/GLIS3	HTT
S14-HTT	F	75	HTT	1.4	PAX8/GLIS3	HTT
S15-HTT	M	57	HTT	1.0	Multiple CNA	Follicular adenoma with spindle cells
S16-HTT	M	80	HTT	5.5	HRAS p.Q61R	Hürthle cell adenoma
S17-HTT	F	66	HTT	0.4	Multiple CNA	PTC, solid variant

F, female; M, male; HTT, hyalinizing trabecular tumor; PTC, papillary thyroid carcinoma; CNA, copy number alterations.

other mutations, indicating that all identified molecular alterations are somatic events (Fig. 2).

Next, to confirm the fusions at the chromosomal level, fluorescence *in situ* hybridization (FISH) was performed with DNA probes corresponding to the *PAX8* and *GLIS3* and *PAX8* and *GLIS1* chromosomal regions. The hybridized tumor cell nuclei demonstrated one pair of fused signals in the majority of cells, confirming the occurrence of interchromosomal rearrangements leading to *PAX8–GLIS3* and *PAX8–GLIS1* fusions (Fig. 1D and E).

Histopathological review of tumors

Histological slides from all 17 cases with the initial diagnosis of HTT were reviewed by three thyroid pathologists blinded to the results of molecular analysis. The histologic diagnosis of HTT was confirmed in 14 cases. All of these tumors were positive for a *GLIS* rearrangement, including 13 (93%) *PAX8–GLIS3* fusions and one (7%) *PAX8–GLIS1* fusion (Table 1). The tumors were well circumscribed and had a thin or moderately thick fibrous capsule as shown in Figure 3A (For digital images of all tumors, see http://image.upmc.edu:8080/Nikiforov%20HTT%20study/view.apml opened via WebScope). None of the cases showed capsular or vascular invasion. The tumors had a prominent trabecular architecture characteristic of HTT with straight or curvilinear bands of tumor cells (Fig. 3B–D). Abundant dense intratrabecular, heavily hyalinized stroma surrounding tumor cells was seen (Fig. 3C). The cells had a polygonal shape, with copious pale to eosinophilic cytoplasm. Cytoplasmic

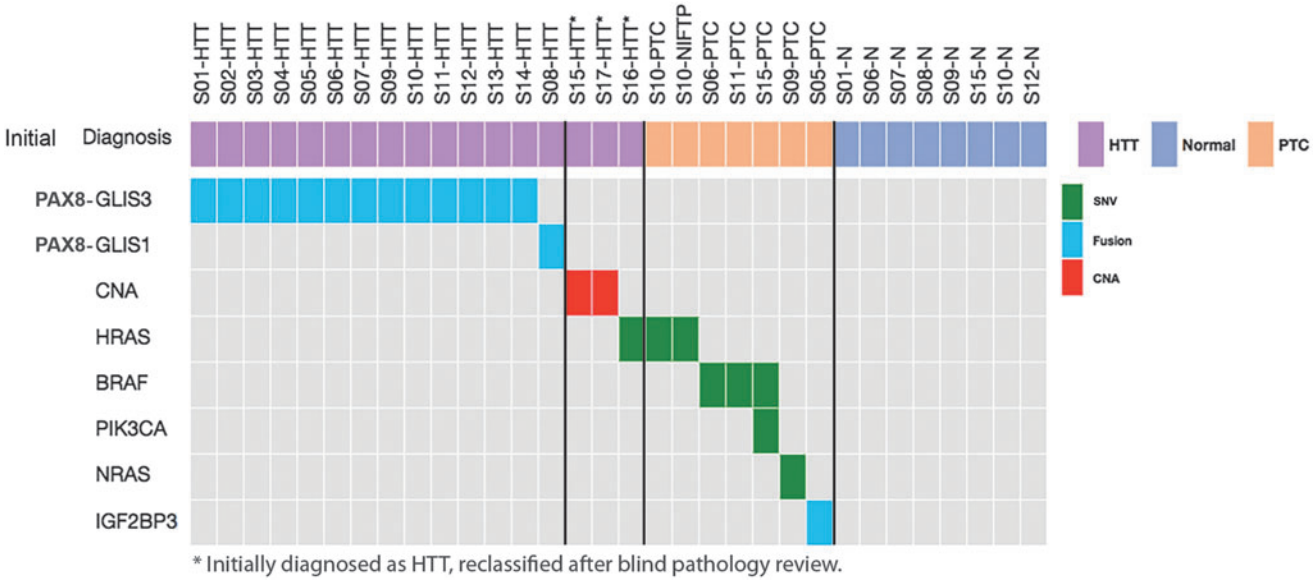

FIG. 2. Summary of molecular alterations detected among 17 tumors initially diagnosed as HTT and in co-existing other tumors and normal thyroid tissue. PTC, papillary thyroid carcinoma; CNA, copy number alterations.

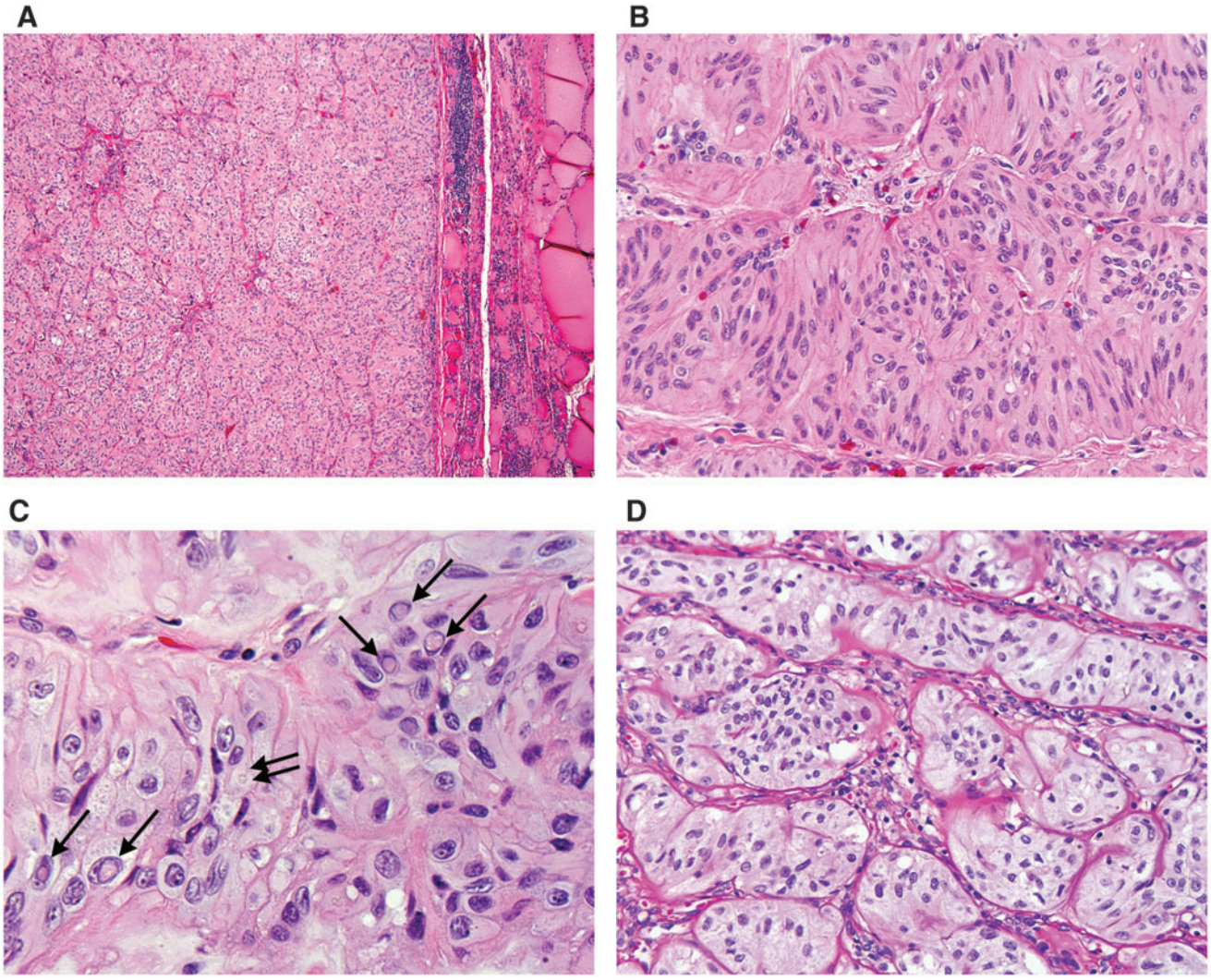

FIG. 3. Histopathologic features of HTT carrying *PAX8–GLIS3* (**A**–**C**) and *PAX8–GLIS1* (**D**) fusions. (**A**) Low-power view showing a well delineated tumor-normal interface with thin fibrotic capsule. (**B**) Medium-power view showing trabecular architecture with straight to curvilinear bands of tumor cells with elongated nuclei arranged perpendicular to the long axis of the trabeculae and abundant intra-trabecular hyalinized stroma. (**C**) High-power view showing tumor cells within trabeculae with irregular nuclear contours, abundant nuclear pseudoinclusions (arrows), and occasional nuclear grooves. A yellow body is seen in the cytoplasm (double arrow). Abundant hyalinization is seen as deposition of homogeneous pinkish material within trabeculae. (**D**) Prominent trabecular architecture in the tumor positive for *PAX8–GLIS1* fusions. See full digital images of representative tumor sections at http://image.upmc.edu:8080/Nikiforov%20HTT%20study/view.apml opened via WebScope.

yellow bodies could be found in most cases (Fig. 3C). The nuclei of the tumor cells had an oval to elongated shape and showed nuclear features overlapping with those of PTC, as characteristically seen in HTT. Those included irregular nuclear contours and abundant intra-nuclear grooves and pseudoinclusions. The latter were particularly prominent in virtually every tumor, with two to five cells with nuclear pseudoinclusions seen in one high-power microscopic field (Fig. 3C). Mitotic figures were rare, typically <1 per 10 high-power fields (400×).

In three tumors with the initial diagnosis of HTT, this diagnosis was not confirmed on blind review. These tumors had a smooth, noninvasive border with variably thick capsules and a vague trabecular architecture with some stromal hyalinization, which prompted the initial diagnosis of HTT, but lacked a pronounced trabecular architecture, intra-trabecular hyalinization, and abundance of nuclear pseudoinclusions expected in HTT (Fig. 4; see http://image.upmc.edu:8080/Nikiforov%20HTT%20study/view.apml). Of those cases, one was reclassified as follicular adenoma with spindle cells, one as Hürthle cell adenoma, and one as solid variant PTC (Table 1). After unblinding, none of these three tumors was positive for *GLIS* fusions. Instead, they harbored genetic alterations found in thyroid adenomas and carcinomas (Fig. 2).

As a result, among tumors possessing all classical microscopic features of HTT, all 14 had *GLIS* fusions.

Functional consequences of GLIS rearrangements

The identified rearrangements involve fusions of *PAX8* with either the *GLIS3* or *GLIS1* genes. PAX8 is a paired box transcription factor, which is highly expressed in

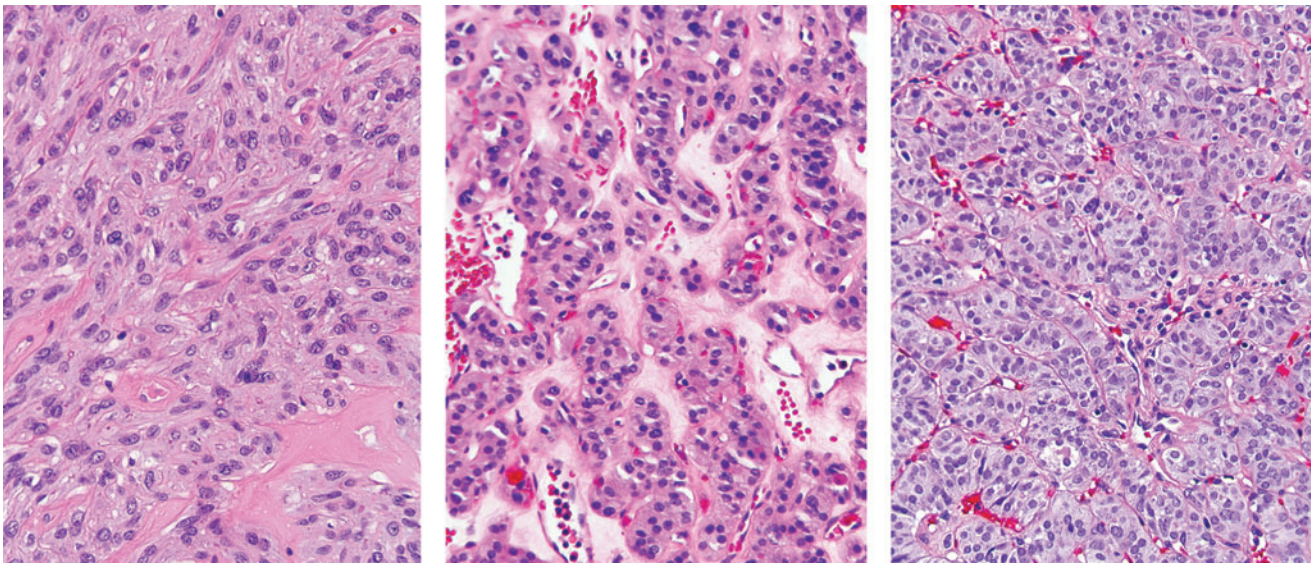

FIG. 4. Histopathologic features of *GLIS* fusion-negative tumors initially diagnosed as HTT and reclassified on blind review by a panel of thyroid pathologists. *Left:* This tumor (S15-HTT) composed of mostly spindle cells arranged in solid sheets with focal stromal hyalinization was reclassified as follicular adenoma with spindle cells. *Center:* This tumor (S16-HTT) with predominantly microfollicular architecture, cells with abundant granular cytoplasm, and stromal hyalinization was reclassified as Hürthle cell adenoma. *Right:* This tumor (S17-HTT) with solid and trabecular architecture and no hyalinization but moderately developed nuclear features of PTC was reclassified as solid variant of PTC. See full digital images of representative tumor sections at http://image.upmc.edu:8080/Nikiforov%20HTT%20study/view.apml opened via WebScope.

differentiated thyroid follicular cells and required for normal thyroid development and function (52). GLI-similar 1 and 3 (GLIS1 and GLIS3) belong to a family of the GLI-similar zinc finger transcription factors that can act either as activators or repressors of gene transcription, and in thyroid, GLIS3 is known to be an important regulator of thyroid hormone biosynthesis (53,54). GLIS1 and GLIS3 share a highly homologous DNA-binding domain that consists of five zinc finger motifs (55). The DNA-binding domain is coded by exons 4–6 of *GLIS3* and exons 3–5 of *GLIS1*. The *PAX8–GLIS3* and *PAX8–GLIS1* fusions juxtapose exon 3 of *GLIS3* or exon 2 of *GLIS1* in-frame and downstream of exon 2 of *PAX8*. As a result, the chimeric transcripts should be regulated by the *PAX8* gene promoter and preserve the zinc-finger containing DNA-binding domains of both *GLIS* genes.

The predicted structure of *PAX8–GLIS3* and *PAX8–GLIS1* transcripts was confirmed by RNA-Seq data. They showed high levels of expression of exons 3–10 of GLIS3 in the chimeric *PAX8–GLIS3* transcript in tumors compared to the normal thyroid tissue (Fig. 5A). PAX8 had a similar level of expression in the tumor and normal samples. Overall, compared to normal thyroid tissues ($n = 16$), the *PAX8–GLIS3*-positive HTT ($n = 7$) showed a 6.8-fold increase (range 3.6- to 58.4-fold) in *GLIS3* mRNA expression (Fig. 5B). Similarly, a tumor carrying a *PAX8–GLIS1* fusion showed a 20.2-fold increase in *GLIS1* mRNA compared to normal thyroid tissues. Further, overexpression of the GLIS3 protein was demonstrated in HTT tissue sections by immunohistochemistry with an antibody to the C-terminus region of human GLIS3, with immunoreactivity observed both in the tumor cell nuclei and the cytoplasm (Fig. 5C).

To obtain further insights into the impact of *PAX8–GLIS3* fusion on thyroid cell function, we used the RNA-Seq gene expression data from GLIS-fused HTTs and normal thyroid tissues to perform pathway analysis using several pathway enrichment programs (KEGG, Reactome, and Gene Ontology (GO) biological process analysis; Supplementary Table S4A–CS). The analysis revealed dysregulation of multiple pathways, with extracellular matrix–related (ECM-related) and thyroid hormone biosynthesis and ion transmembrane transport (TH-related) pathways being among the top pathways dysregulated in tumors with *PAX8–GLIS3* as compared to normal thyroid tissue (Fig. 6A and Supplementary Table S5). A number of extracellular matrix-related genes, including the majority of collagen genes, such as *COL4A1*, *COL5A3*, *COL5A2*, *COL15A1*, and *COL1A2*, were expressed at significantly higher levels in HTT as compared to normal thyroid tissue (Supplementary Table S5 and Supplementary Fig. S2). Overexpression and deposition of collagens in the areas corresponding to intra-trabecular hyalinization seen in HTT was confirmed by immunohistochemistry with collagen IV and a pan-collagen antibodies (Fig. 6B and C).

Among genes related to thyroid hormone biosynthesis, *SLC16A2* (MCT8) and *SLC5A5* (NIS) were significantly upregulated and *TSHR*, *TPO*, and deiodinase genes (*DIO1*, *DIO2*) were downregulated (Supplementary Table S5 and Supplementary Fig. S3).

Molecular profiling of synchronous PTC

HTTs are known to co-occur in thyroid glands that, not infrequently, also have PTC and other nodular lesions (20). Indeed, in the series of HTT cases, six coexisting PTC and one noninvasive follicular thyroid neoplasm with papillary-like nuclear features (NIFTP) present in the same or opposite thyroid lobe were identified. These tumors were genotyped for the known thyroid tumor alterations using a 112-gene targeted NGS panel (51). All synchronous PTC and a NIFTP

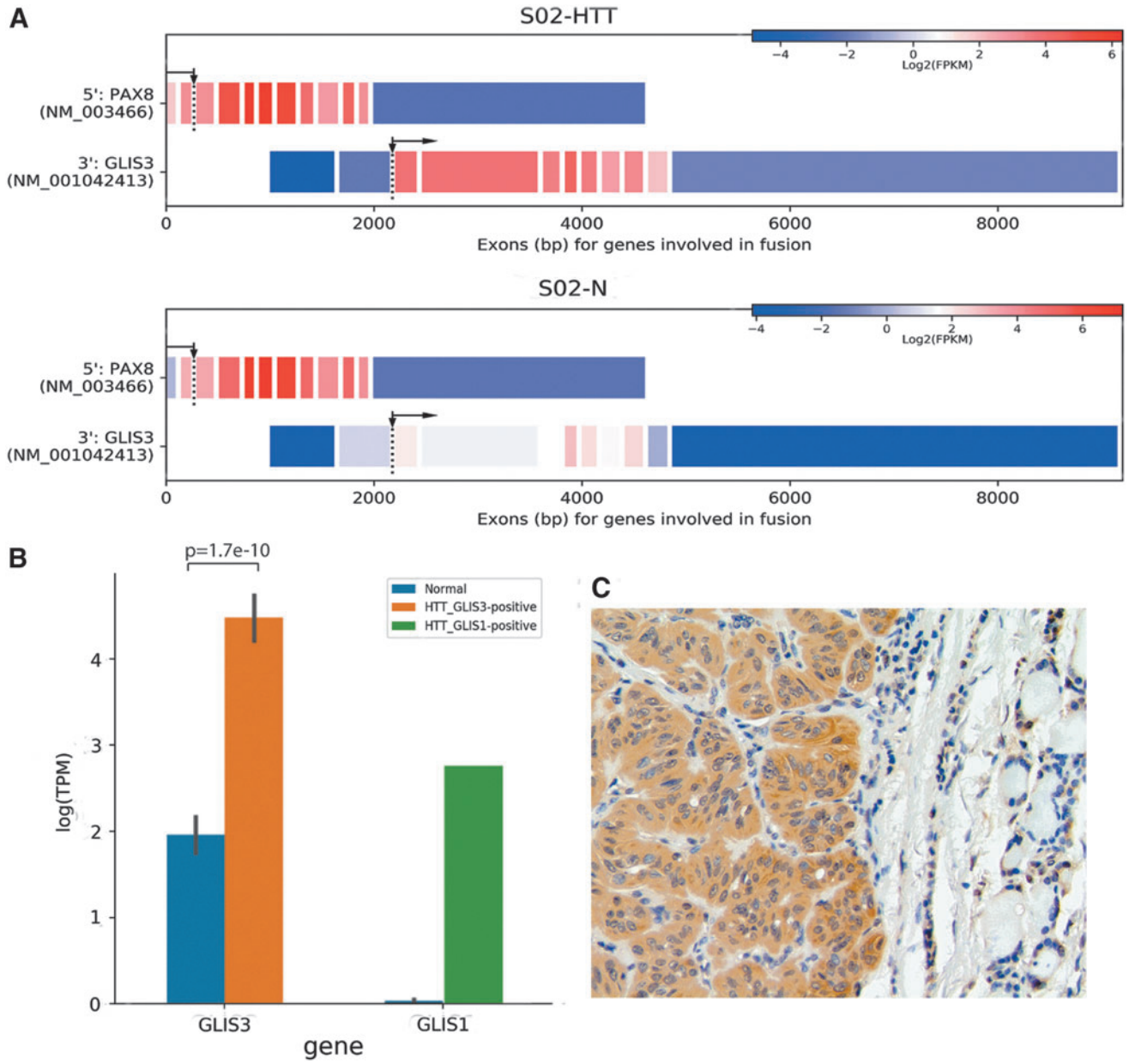

FIG. 5. Consequences of *PAX8–GLIS* fusions on expression of GLIS3 and GLIS1. (**A**) Expression levels of the individual PAX8 and GLIS3 exons in the *PAX8–GLIS3* fusion-positive HTT and corresponding normal tissue based on RNA-Seq data. Exons 3–10 of GLIS3 are highly expressed in the tumor as compared to normal tissue. (**B**) Expression of GLIS3 and GLIS1 mRNA in GLIS-rearranged tumors compared to a pool of 16 normal thyroid tissues ($M \pm SD$). (**C**) Immunohistochemistry with an antibody to the C-terminus region of GLIS3 showing strong nuclear and cytoplasmic staining in the HTT cells and patchy staining of individual cells in adjacent normal thyroid tissue (right). *SD*, standard deviation.

case were negative for *GLIS* fusions. However, they were all positive for other alterations, including the $BRAF^{V600E}$ mutation in two PTC, a $BRAF^{V600E}$ and *PIK3CA* in one PTC, an $NRAS^{Q61R}$ mutation in one PTC, a *THADA–IGF2BP3* fusion in one PTC, and an identical $HRAS^{G13R}$ mutation in both a PTC and a NIFTP coexisting in the same thyroid gland (Fig. 2).

Prevalence of GLIS fusions in PTC and thyroid nodules

In order to evaluate the prevalence of *PAX8–GLIS3* and *PAX8–GLIS1* fusions in PTC, 220 samples of PTC by RT-PCR were studied. This set of tumors included 111 freshly frozen samples of unselected PTC and 109 FFPE samples of preselected aggressive PTC. In addition, The Cancer Genome Atlas (TCGA) data on 484 PTC tested for fusions using RNA-Seq were reviewed (56). No *PAX8–GLIS3* fusion was found among the 220 tumor samples (Supplementary Figs. S5 and S6) and in the TCGA study (Table 2). However, a *PAX8–GLIS1* fusion was identified in 1/111 tumors from the unselected PTC cohort (Supplementary Figs. S4 and S5). No *PAX8–GLIS1* fusion was found among 109 samples from the aggressive PTC cohort or 484 PTC in TCGA study. Histologic slides from the tumor positive for *PAX8–GLIS1* were reviewed and revealed

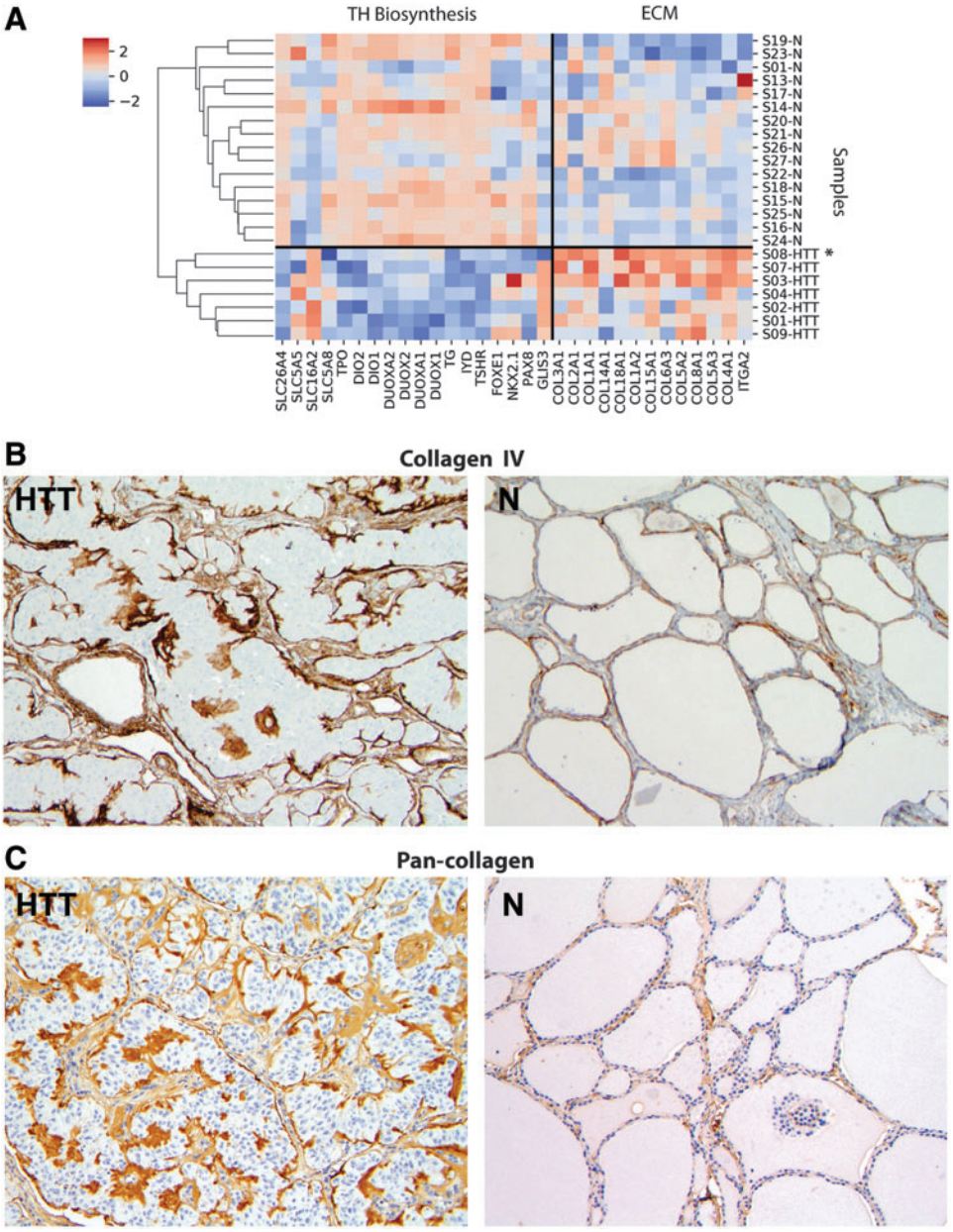

FIG. 6. Dysregulation of extracellular matrix (ECM)-related and thyroid hormone biosynthesis and ion transmembrane transport-related pathways in *GLIS*-rearranged HTT. (**A**) Heatmap generated from gene expression profiles obtained by RNA-Seq for ECM pathways and thyroid hormone (TH) biosynthesis pathway shows separate clusters for normal tissue and HTT GLIS fusion-positive cases. In the ECM pathway, the majority of collagen genes show upregulation compared to normal thyroid tissue. In the TH biosynthesis pathway, high expression of the *SLC16A2* (MCT8) and *SLC5A5* (NIS) genes and low *TSHR*, *TPO*, and deiodinase genes was detected. Of note, case S08-HTT* is positive for *PAX8–GLIS1* fusion and therefore shows no GLIS3 expression. (**B** and **C**) Immunohistochemistry with collagen IV (**B**) and pan-collagen antibodies (**C**) showing massive lumpy depositions of collagen in HTT compared to adjacent normal thyroid tissues (N).

an encapsulated tumor with predominantly solid and microfollicular architecture and only a focal trabecular pattern composed of cells with moderately developed nuclear features of PTC but highly abundant nuclear pseudoinclusions seen in focal areas (Supplementary Fig. S4). Despite a somewhat unusual appearance, the diagnosis of PTC was confirmed. Interestingly, the microscopic appearance of the tumor, as well as patient demographics, were identical between this case and a thyroid tumor positive for *PAX8–GLIS1* fusion in the expanded TCGA PanCancer Atlas study (tumor case # TCGA-BJ-A291,

Table 2. Prevalence of *PAX8–GLIS3* and *PAX8–GLIS1* Fusions in the Current Study and TCGA Cohort

		PTC			
Fusion type	*HTT, current study* (n = *14*)	*TCGA study*[a] (n = *484*)	*Current study, unselected PTC* (n = *111*)	*Current study, aggressive PTC* (n = *109*)	*Total*
PAX8–GLIS3	13/14 (93%)	0/484	0/111	0/109	0/704 (0.0%)
PAX8–GLIS1	1/14 (7%)	0/484	1[b]/111	0/109	1/704 (0.1%)

[a]As reported by TCGA Research Network (56).
[b]The same case was reported as *PAX8/GLIS1* positive in TCGA PanCancer Atlas study (see www.cbioportal.org/).
TCGA, The Cancer Genome Atlas.

contributed from the University of Pittsburgh Medical Center), suggesting that it may represent the same tumor.

Finally, taking advantage of the fact that *PAX8–GLIS3* fusion is detectable by the ThyroSeq v3 GC panel, the prevalence of this fusion was evaluated in 10,165 consecutive FNA samples from thyroid nodules with indeterminate cytology. *PAX8–GLIS3* was detected in eight ($\sim$0.1%) of the nodules. Surgical follow-up was available for five of these patients, and all five nodules carrying *PAX8–GLIS3* were pathologically diagnosed as HTT after excision.

Clinical features and follow-up for patients with HTT

All 14 patients with HTT were female, with a mean age of 57 years (range 31–75 years). The mean size of resected HTT was 1.6 cm (range 0.6–3.5 cm). Preoperative ultrasound was performed for six patients; five (83%) HTT nodules were solid/hypoechoic, and three (50%) were hypervascular. FNA cytology was reported as positive for malignancy (Bethesda VI) in one case, suspicious for malignancy (Bethesda V) in two cases, follicular neoplasm/suspicious for follicular neoplasm (Bethesda IV) in two cases, and atypia of undetermined significance/follicular lesion of undetermined significance (Bethesda III) in one case. Clinical follow-up was available for 9/14 patients with *GLIS* fusion-positive HTT. There were no tumor recurrences after a mean follow-up of 65 months (range 4–181 months). Radioactive iodine was administered to two patients and recommended to one patient for concurrent PTC.

Discussion

This study uncovered the underlying genetic mechanism of the thyroid neoplasm known as HTT by demonstrating that gene fusions involving the *PAX8* and *GLIS* genes represent a genetic hallmark of these tumors. In fact, these fusions, typically *PAX8–GLIS3*, were identified in 100% of tumors that had fully developed histological features of HTT.

Further, the study shows that these tumors have a quiet genome with a low number of somatic mutations and no significant DNA copy number alterations. Furthermore, these tumors have no mutations characteristic of PTC and all of its variants, such as *BRAF* and *RAS* point mutations and *RET/PTC* and other gene fusions. Reciprocally, PTC were found to carry no *PAX8–GLIS3* fusions in a large and well annotated cohort of tumors in this study ($n = 220$) and in TCGA tumor cohort ($n = 484$) (56). Similarly, none of the PTC co-occurring in the same thyroid gland with HTT had a *GLIS* fusion, but instead they carried $BRAF^{V600E}$ and other alterations characteristic of PTC. However, a *PAX8–GLIS1* fusion, which was detected in one HTT, was also found in a tumor that had some microscopic features of HTT but carried a consensus diagnosis of PTC. Overall, the contrasting molecular profiles of HTT and PTC, including tumors arising in the same thyroid gland, argue strongly against biological similarity between these two tumor types.

This study demonstrates that fusions of *GLIS3* or *GLIS1* genes to *PAX8*, formed as a result of inter-chromosomal rearrangements, lead to the generation of chimeric transcripts and strong overexpression of the 3′ portions of the *GLIS* genes with the intact DNA-binding zinc finger domains of these transcription factors. Further, the study found that the *PAX8–GLIS3* fusion-positive tumors show consistent upregulation of expression of extracellular matrix–related genes, including several collagen genes such as *COL4A1*, coding for the alpha-1 subunit of collagen IV found primarily in the basal lamina. Excessive production and deposition of collagen IV and other collagens in these tumors was confirmed by immunohistochemistry. This is likely responsible for producing extensive hyalinization, which results in the characteristic microscopic appearance and name of these tumors. How exactly GLIS regulates the expression of extracellular matrix–related genes remains to be clarified, but such an effect of GLIS is not entirely unexpected. Indeed, *GLIS3* knockout in thyroid cells of mice has been previously shown to lead to significant downregulation of the extracellular matrix genes (54). Abnormal intracellular and extracellular deposition of basement membrane material was demonstrated in these tumors before by electron microscopy and immunohistochemistry using a collagen IV antibody (57,58), although the mechanisms responsible for this phenomenon were not known.

Dysregulation of the thyroid hormone biosynthesis pathway in HTT carrying *GLIS* fusions was also observed, which is also expected based on the known role of GLIS3 in regulating thyroid cell development and function (54). However, specific genes belonging to this pathway were variably affected, as some of them (*SLC16A2/MCT8*, *SLC5A5/NIS*) were upregulated, whereas many other genes coding for proteins involved in thyroid hormone synthesis either were downregulated or had levels of expression similar to normal thyroid tissue.

Whereas the role of GLIS3 in thyroid cell function is well established, little is known about the physiological function of GLIS1 in thyroid cells. GLIS1 and GLIS3 belong to a subfamily of Krüppel-like zinc finger transcription factors that regulate transcription of a variety of genes in physiological and pathological conditions (59). In the thyroid, GLIS3 has been shown to be an important regulator of thyroid hormone synthesis, with loss of GLIS3 function by mutation associated with the development of congenital or neonatal hypothyroidism (53,60). Similarly, strong downregulation of the expression of SLC5A5/NIS and other iodide transporters was observed in thyroid glands of GLIS3-deficient mice (54). The known high homology ($\sim$94%) between the zinc finger DNA-binding domain of *GLIS3* and *GLIS1* (55) and findings in this study of similar effects of overexpression of these two genes through gene fusion on dysregulation of signaling pathways including thyroid hormone biosynthesis raise the question whether *GLIS1* is also involved in regulating certain aspects of thyroid cell function.

In this series of patients and among 118 tumors reported in the largest study to date (20), tumors with histopathologic features of HTT that lack invasion did not have regional or distant metastases at presentation, and patients experienced no tumor recurrence or any other adverse effects on follow-up. Furthermore, no *GLIS* fusions were found in a series of 109 aggressive PTC, including those with distant metastases or extensive local invasion. This suggests that in the absence of invasion, *GLIS* fusion-positive thyroid neoplasms currently known as HTT are benign, as initially suggested by Carney *et al*. (1). Therefore, these tumors should be considered adenomas and classified as ''*GLIS*-rearranged hyalinizing trabecular adenoma.''

The change of the tumor name from more ambiguous ''tumor'' to ''adenoma'' should reflect more accurately the

benign nature of this disease, but it does not exclude the existence of a malignant counterpart of this tumor. In fact, it would closely recapitulate the deeply engraved nomenclature approach in medical practice to thyroid adenoma/thyroid carcinoma tumors that have similar overall morphology but are separated based on the absence or presence of invasion. Single cases of invasive tumors with trabecular growth and hyalinization have been reported, and some manifested with distant metastases (4,5,20). Such tumors can be designated as ''hyalinizing trabecular carcinoma,'' as proposed before (5). However, it remains unclear whether these invasive tumors carry *GLIS* fusions, and at this point in time, both possibilities should be considered. If invasive tumors are found to carry *GLIS* fusions, it would support the designation of these tumors as ''*GLIS*-rearranged hyalinizing trabecular carcinoma'' and provide strong evidence for a biological similarity between these tumors and existence of progression of these tumors with characteristic hyalinization and trabecular growth from adenoma to carcinoma. Alternatively, if invasive tumors with similar histology are found to be *GLIS*-negative but instead carry genetic alterations in classical PTC genes, this would indicate that they represent a peculiar type of PTC and suggest that *GLIS*-positive tumors are likely nonprogressive benign neoplasms.

There is also a possibility that tumors carrying *GLIS3* and *GLIS1* fusions have a different predisposition to malignant transformation. Indeed, current data suggest that progression of *PAX8–GLIS3*-positive tumors would be a very rare event, as these fusions were not identified in >700 carefully curated PTC in TCGA cohort (56) and this study. However, a single case of *PAX8–GLIS3* has been reported in a 1 cm classical PTC that was intrathyroidal and had no invasion (61). The reported mRNA fusion point between exon 2 of *PAX8* and exon 4 of *GLIS3* appears to be different to the one identified in tumors in this study and apparently resulted in an out-of-frame fusion. Furthermore, the histological appearance of the tumor was not illustrated, precluding evaluation for the microscopic features of HTT. The probability of malignant transformation may be higher for tumors with *PAX8–GLIS1* fusion, which was found with low prevalence in HTT, but also one tumor classified as PTC. This tumor had some microscopic features of HTT, particularly a very high number on nuclear pseudoinclusions, but overall had the histological appearance of PTC.

Finally, this study demonstrates that *GLIS* fusions can be detected preoperatively in thyroid FNA samples, and among nodules with indeterminate cytology, primarily Bethesda III and IV, *PAX8–GLIS3* was found in $\sim$0.1% of cases. The prevalence of these fusions in Bethesda V and IV nodules may be even higher, as HTT in more than half of the cases yield a cytological diagnosis of PTC or suspicious for PTC (19,62,63). In fact, due to well expressed nuclear features of PTC, HTT commonly pose a diagnostic difficulty for thyroid cytology and lead to false-positive cytology diagnoses triggering total thyroidectomy (62).

Interestingly, among nodules with a prospectively detected *PAX8–GLIS3* fusion that underwent surgery, 5/5 were diagnosed as HTT on surgical pathology. While the number of cases with prospectively accumulated follow-up is low and further studies are required to reliably establish the probability of malignancy in nodules carrying *PAX8–GLIS3* and *PAX8–GLIS1* fusions, the results of this study suggest that thyroid lobectomy is likely to be an appropriate initial surgical approach for such nodules. Future studies are required to determine if clinically significant cancers carrying these fusions exist, which will help to determine if surgical treatment is needed at all for thyroid nodules carrying *PAX8–GLIS3* or any type of *GLIS* fusion.

Acknowledgments

We thank Mrs. Jessica Tebbets for her help in preparation of this manuscript and for collection of follow-up information. This work was supported in part by the NIH grants R01CA181150 and P50CA097190. Sample collection was supported in part by the UPCI Tissue and Research Pathology/Health Sciences Tissue Bank shared resource which is supported in part by award P30CA047904 and by a generous gift from William and Susan Johnson.

Author Disclosure Statement

M.N.N. and Y.E.N. receive compensation from their employer in connection with ThyroSeq test offered through CBLPath/Sonic Healthcare USA; they own intellectual property related to the ThyroSeq test. The remaining authors have nothing to disclose.

References

1. Carney JA, Ryan J, Goellner JR 1987 Hyalinizing trabecular adenoma of the thyroid gland. Am J Surg Pathol **11:** 583–591.
2. Bronner MP, LiVolsi VA, Jennings TA 1988 PLAT: paraganglioma-like adenomas of the thyroid. Surg Pathol **1:** 383–389.
3. Sambade C, Franssila K, Cameselle-Teijeiro J, Nesland J, Sobrinho Simoes M 1991 Hyalinizing trabecular adenoma: a misnomer for a peculiar tumor of the thyroid gland. Endocr Pathol **2:**83–91.
4. González-Cámpora R, Fuentes-Vaamonde E, Hevia-Vázquez A, Otal-Salaverri C, Villar-Rodriguez JL, Galera-Davidson H 1998 Hyalinizing trabecular carcinoma of the thyroid gland: report of two cases of follicular cell thyroid carcinoma with hyalinizing trabecular pattern. Ultrastruct Pathol **22:**39–46.
5. Molberg K, Albores-Saavedra J 1994 Hyalinizing trabecular carcinoma of the thyroid gland. Hum Pathol **25:** 192–197.
6. Gowrishankar S, Pai SA, Carney JA 2008 Hyalinizing trabecular carcinoma of the thyroid gland. Histopathology **52:**529–531.
7. DeLellis RA, Lloyd RV, Heitz PU, Eng C (eds) 2004 World Health Organization Classification of Tumours. Pathology and Genetics of Tumours of Endocrine Organs. IARC Press, Lyon, France.
8. Lloyd RV, Osamura RY, Klöppel G, Rosai J (eds) 2017 World Health Organization Classification of Tumours of Endocrine Organs. Fourth edition. IARC Press, Lyon, France.
9. Cheung CC, Boerner SL, MacMillan CM, Ramyar L, Asa SL 2000 Hyalinizing trabecular tumor of the thyroid: a variant of papillary carcinoma proved by molecular genetics. Am J Surg Pathol **24:**1622–1626.
10. Papotti M, Volante M, Giuliano A, Fassina A, Fusco A, Bussolati G, Santoro M, Chiappetta G 2000 *RET/PTC*

activation in hyalinizing trabecular tumors of the thyroid. Am J Surg Pathol **24:**1615–1621.
11. Lloyd RV 2002 Hyalinizing trabecular tumors of the thyroid: a variant of papillary carcinoma? Adv Anat Pathol **9:**7–11.
12. Sheu SY, Vogel E, Worm K, Grabellus F, Schwertheim S, Schmid KW 2010 Hyalinizing trabecular tumour of the thyroid-differential expression of distinct miRNAs compared with papillary thyroid carcinoma. Histopathology **56:** 632–640.
13. Salvatore G, Chiappetta G, Nikiforov YE, Decaussin-Petrucci M, Fusco A, Carney JA, Santoro M 2005 Molecular profile of hyalinizing trabecular tumours of the thyroid: high prevalence of *RET*/*PTC* rearrangements and absence of *B-raf* and *N-ras* point mutations. Eur J Cancer **41:**816–821.
14. Nakamura N, Carney JA, Jin L, Kajita S, Pallares J, Zhang H, Qian X, Sebo TJ, Erickson LA, Lloyd RV 2005 RASSF1A and NORE1A methylation and *BRAFV600E* mutations in thyroid tumors. Lab Invest **85:**1065–1075.
15. Baloch ZW, Puttaswamy K, Brose M, LiVolsi VA 2006 Lack of *BRAF* mutations in hyalinizing trabecular neoplasm. CytoJournal **3:**17.
16. Kim T, Oh YL, Kim KM, Shin JH 2011 Diagnostic dilemmas of hyalinizing trabecular tumours on fine needle aspiration cytology: a study of seven cases with *BRAF* mutation analysis. Cytopathology **22:**407–413.
17. Lee S, Han BK, Ko EY, Oh YL, Choe JH, Shin JH 2011 The ultrasonography features of hyalinizing trabecular tumor of the thyroid are more consistent with its benign behavior than cytology or frozen section readings. Thyroid **21:**253–259.
18. Capella G, Matias-Guiu X, Ampudia X, de Leiva A, Perucho M, Prat J 1996 *Ras* oncogene mutations in thyroid tumors: polymerase chain reaction-restriction-fragment-length polymorphism analysis from paraffin-embedded tissues. Diagn Mol Pathol **5:**45–52.
19. Jang H, Park CK, Son EJ, Kim EK, Kwak JY, Moon HJ, Yoon JH 2016 Hyalinizing trabecular tumor of the thyroid: diagnosis of a rare tumor using ultrasonography, cytology, and intraoperative frozen sections. Ultrasonography **35:** 131–139.
20. Carney JA, Hirokawa M, Lloyd RV, Papotti M, Sebo TJ 2008 Hyalinizing trabecular tumors of the thyroid gland are almost all benign. Am J Surg Pathol **32:**1877–1889.
21. Roy S, LaFramboise WA, Liu TC, Cao D, Luvison A, Miller C, Lyons MA, O'Sullivan RJ, Zureikat AH, Hogg ME, Tsung A, Lee KK, Bahary N, Brand RE, Chennat JS, Fasanella KE, McGrath K, Nikiforova MN, Papachristou GI, Slivka A, Zeh HJ, Singhi AD 2018 Loss of chromatin-remodeling proteins and/or CDKN2A associates with metastasis of pancreatic neuroendocrine tumors and reduced patient survival times. Gastroenterology **154:**2060–2063.e8.
22. Li H, Durbin R 2010 Fast and accurate long-read alignment with Burrows–Wheeler transform. Bioinformatics **26:**589–595.
23. Li H, Handsaker B, Wysoker A, Fennell T, Ruan J, Homer N, Marth G, Abecasis G, Durbin R; 1000 Genome Project Data Processing Subgroup 2009 The Sequence Alignment/Map format and SAMtools. Bioinformatics **25:**2078–2079.
24. McKenna A, Hanna M, Banks E, Sivachenko A, Cibulskis K, Kernytsky A, Garimella K, Altshuler D, Gabriel S, Daly M, DePristo MA 2010 The Genome Analysis Toolkit: a MapReduce framework for analyzing next-generation DNA sequencing data. Genome Res **20:**1297–1303.
25. Koboldt DC, Zhang Q, Larson DE, Shen D, McLellan MD, Lin L, Miller CA, Mardis ER, Ding L, Wilson RK 2012 VarScan 2: somatic mutation and copy number alteration discovery in cancer by exome sequencing. Genome Res **22:**568–576.
26. Fang H, Bergmann EA, Arora K, Vacic V, Zody MC, Iossifov I, O'Rawe JA, Wu Y, Jimenez Barron LT, Rosenbaum J, Ronemus M, Lee YH, Wang Z, Dikoglu E, Jobanputra V, Lyon GJ, Wigler M, Schatz MC, Narzisi G 2016 Indel variant analysis of short-read sequencing data with Scalpel. Nat Protoc **11:**2529–2548.
27. Hart RK, Rico R, Hare E, Garcia J, Westbrook J, Fusaro VA 2015 A Python package for parsing, validating, mapping and formatting sequence variants using HGVS nomenclature. Bioinformatics **31:**268–270.
28. Wang K, Li M, Hakonarson H 2010 ANNOVAR: functional annotation of genetic variants from high-throughput sequencing data. Nucleic Acids Res **38:**e164.
29. Genomes Project C, Auton A, Brooks LD, Durbin RM, Garrison EP, Kang HM, Korbel JO, Marchini JL, McCarthy S, McVean GA, Abecasis GR 2015 A global reference for human genetic variation. Nature **526:**68–74.
30. Lek M, Karczewski KJ, Minikel EV, Samocha KE, Banks E, Fennell T, O'Donnell-Luria AH, Ware JS, Hill AJ, Cummings BB, Tukiainen T, Birnbaum DP, Kosmicki JA, Duncan LE, Estrada K, Zhao F, Zou J, Pierce-Hoffman E, Berghout J, Cooper DN, Deflaux N, DePristo M, Do R, Flannick J, Fromer M, Gauthier L, Goldstein J, Gupta N, Howrigan D, Kiezun A, Kurki MI, Moonshine AL, Natarajan P, Orozco L, Peloso GM, Poplin R, Rivas MA, Ruano-Rubio V, Rose SA, Ruderfer DM, Shakir K, Stenson PD, Stevens C, Thomas BP, Tiao G, Tusie-Luna MT, Weisburd B, Won HH, Yu D, Altshuler DM, Ardissino D, Boehnke M, Danesh J, Donnelly S, Elosua R, Florez JC, Gabriel SB, Getz G, Glatt SJ, Hultman CM, Kathiresan S, Laakso M, McCarroll S, McCarthy MI, McGovern D, McPherson R, Neale BM, Palotie A, Purcell SM, Saleheen D, Scharf JM, Sklar P, Sullivan PF, Tuomilehto J, Tsuang MT, Watkins HC, Wilson JG, Daly MJ, MacArthur DG; Exome Aggregation Consortium 2016 Analysis of protein-coding genetic variation in 60,706 humans. Nature **536:**285–291.
31. Adzhubei I, Jordan DM, Sunyaev SR 2013 Predicting functional effect of human missense mutations using PolyPhen-2. Curr Protoc Hum Genet Chaper 7:Unit7.20.
32. Ng PC, Henikoff S 2003 SIFT: predicting amino acid changes that affect protein function. Nucleic Acids Res **31:** 3812–3814.
33. Forbes SA, Beare D, Boutselakis H, Bamford S, Bindal N, Tate J, Cole CG, Ward S, Dawson E, Ponting L, Stefancsik R, Harsha B, Kok CY, Jia M, Jubb H, Sondka Z, Thompson S, De T, Campbell PJ 2017 COSMIC: somatic cancer genetics at high-resolution. Nucleic Acids Res **45:** D777–D783.
34. Sherry ST, Ward MH, Kholodov M, Baker J, Phan L, Smigielski EM, Sirotkin K 2001 dbSNP: the NCBI database of genetic variation. Nucleic Acids Res **29:** 308–311.
35. Landrum MJ, Lee JM, Benson M, Brown G, Chao C, Chitipiralla S, Gu B, Hart J, Hoffman D, Hoover J, Jang W, Katz K, Ovetsky M, Riley G, Sethi A, Tully R, Villamarin-Salomon R, Rubinstein W, Maglott DR 2016 ClinVar: public archive of interpretations of clinically relevant variants. Nucleic Acids Res **44:**D862–868.

36. Shen R, Seshan VE 2016 FACETS: allele-specific copy number and clonal heterogeneity analysis tool for high-throughput DNA sequencing. Nucleic Acids Res **44:**e131.
37. Talevich E, Shain AH, Botton T, Bastian BC 2016 CNVkit: genome-wide copy number detection and visualization from targeted DNA sequencing. PLoS Comput Biol **12:**e1004873.
38. Li H, Ruan J, Durbin R 2008 Mapping short DNA sequencing reads and calling variants using mapping quality scores. Genome Res **18:**1851–1858.
39. Iyer MK, Chinnaiyan AM, Maher CA 2011 ChimeraScan: a tool for identifying chimeric transcription in sequencing data. Bioinformatics **27:**2903–2904.
40. Trapnell C, Pachter L, Salzberg SL 2009 TopHat: discovering splice junctions with RNA-Seq. Bioinformatics **25:** 1105–1111.
41. Huret JL, Ahmad M, Arsaban M, Bernheim A, Cigna J, Desangles F, Guignard JC, Jacquemot-Perbal MC, Labarussias M, Leberre V, Malo A, Morel-Pair C, Mossafa H, Potier JC, Texier G, Viguie F, Yau Chun Wan-Senon S, Zasadzinski A, Dessen P 2013 Atlas of genetics and cytogenetics in oncology and haematology in 2013. Nucl Acids Res **41:**D920–924.
42. Akagi K, Suzuki T, Stephens RM, Jenkins NA, Copeland NG 2004 RTCGD: retroviral tagged cancer gene database. Nucl Acids Res **32:**D523–527.
43. Futreal PA, Coin L, Marshall M, Down T, Hubbard T, Wooster R, Rahman N, Stratton MR 2004 A census of human cancer genes. Nat Rev **4:**177–183.
44. Li B, Dewey CN 2011 RSEM: accurate transcript quantification from RNA-Seq data with or without a reference genome. BMC Bioinformatics **12:**323.
45. Liao Y, Smyth GK, Shi W 2014 featureCounts: an efficient general purpose program for assigning sequence reads to genomic features. Bioinformatics **30:**923–930.
46. Robinson MD, McCarthy DJ, Smyth GK 2010 edgeR: a Bioconductor package for differential expression analysis of digital gene expression data. Bioinformatics **26:** 139–140.
47. Kanehisa M, Goto S 2000 KEGG: kyoto encyclopedia of genes and genomes. Nucl Acids Res **28:**27–30.
48. Joshi-Tope G, Gillespie M, Vastrik I, D'Eustachio P, Schmidt E, de Bono B, Jassal B, Gopinath GR, Wu GR, Matthews L, Lewis S, Birney E, Stein L 2005 Reactome: a knowledgebase of biological pathways. Nucl Acids Res **33:** D428–432.
49. Jiao X, Sherman BT, Huang da W, Stephens R, Baseler MW, Lane HC, Lempicki RA 2012 DAVID-WS: a stateful web service to facilitate gene/protein list analysis. Bioinformatics **28:**1805–1806.
50. Julious SA 2004 Sample sizes for clinical trials with normal data. Stat Med **23:**1921–1986.
51. Nikiforova MN, Mercurio S, Wald AI, Barbi de Moura M, Callenberg K, Santana-Santos L, Gooding WE, Yip L, Ferris RL, Nikiforov YE 2018 Analytical performance of the ThyroSeq v3 genomic classifier for cancer diagnosis in thyroid nodules. Cancer **124:**1682–1690.
52. Fernandez LP, Lopez-Marquez A, Santisteban P 2015 Thyroid transcription factors in development, differentiation and disease. Nat Rev **11:**29–42.
53. Dimitri P 2017 The role of GLIS3 in thyroid disease as part of a multisystem disorder. Best Pract Res Clin Endocrinol Metab **31:**175–182.
54. Kang HS, Kumar D, Liao G, Lichti-Kaiser K, Gerrish K, Liao XH, Refetoff S, Jothi R, Jetten AM 2017 GLIS3 is indispensable for TSH/TSHR-dependent thyroid hormone biosynthesis and follicular cell proliferation. J Clin Invest **127:**4326–4337.
55. Lee SY, Noh HB, Kim HT, Lee KI, Hwang DY 2017 Glis family proteins are differentially implicated in the cellular reprogramming of human somatic cells. Oncotarget **8:** 77041–77049.
56. Cancer Genome Atlas Research Network 2014 Integrated genomic characterization of papillary thyroid carcinoma. Cell **159:**676–690.
57. Katoh R, Kakudo K, Kawaoi A 1999 Accumulated basement membrane material in hyalinizing trabecular tumors of the thyroid. Mod Pathol **12:**1057–1061.
58. Li M, Carcangiu ML, Rosai J 1997 Abnormal intracellular and extracellular distribution of basement membrane material in papillary carcinoma and hyalinizing trabecular tumors of the thyroid: implication for deregulation of secretory pathways. Hum Pathol **28:**1366–1372.
59. Jetten AM 2018 GLIS1-3 transcription factors: critical roles in the regulation of multiple physiological processes and diseases. Cell Mol Life Sci **75:**3473–3494.
60. Senee V, Chelala C, Duchatelet S, Feng D, Blanc H, Cossec JC, Charon C, Nicolino M, Boileau P, Cavener DR, Bougneres P, Taha D, Julier C 2006 Mutations in GLIS3 are responsible for a rare syndrome with neonatal diabetes mellitus and congenital hypothyroidism. Nat Genet **38:** 682–687.
61. Yoo SK, Lee S, Kim SJ, Jee HG, Kim BA, Cho H, Song YS, Cho SW, Won JK, Shin JY, Park do J, Kim JI, Lee KE, Park YJ, Seo JS 2016 Comprehensive analysis of the transcriptional and mutational landscape of follicular and papillary thyroid cancers. PLoS Genet **12:**e1006239.
62. Saglietti C, Piana S, La Rosa S, Bongiovanni M 2017 Hyalinizing trabecular tumour of the thyroid: fine-needle aspiration cytological diagnosis and correlation with histology. J Clin Pathol **70:**641–647.
63. Casey MB, Sebo TJ, Carney JA 2004 Hyalinizing trabecular adenoma of the thyroid gland: cytologic features in 29 cases. Am J Surg Pathol **28:**859–867.

Address correspondence to:
Yuri E. Nikiforov, MD, PhD
Department of Pathology
University of Pittsburgh
3477 Euler Way, Room 8031
Pittsburgh, PA 15213

E-mail: nikiforovye@upmc.edu